Charge Density Wave Pinning and Disorder in Two Dimensions†

Hongjie Dai and Charles M. Lieber*

Department of Chemistry and Division of Applied Sciences, Harvard University, Cambridge, Massachusetts 02138

Received: September 22, 1992; In Final Form: October 23, 1992

The structures of the two-dimensional incommensurate charge density wave (CDW) in Nb-doped 1T-TaS_2 ($Nb_xTa_{1-x}S_2$) have been elucidated by scanning tunneling microscopy and quantitative image analysis procedures. Analyses of the STM images demonstrate that Nb impurities introduce topological defects, dislocations, into the CDW lattice. Quantitative analysis of the density of dislocations and comparisons of this data with theoretical scaling arguments demonstrate unambiguously that the pinning of the CDW by Nb impurities is weak. In addition, the structure factor, radial distribution function, and translational and orientational correlation functions have been investigated as a function of impurity concentration. Calculations of the translational correlation function demonstrate that translational order decays exponentially over several lattice constants for $x(Nb) > 0$. In contrast, calculations of the orientational correlation function show that the orientational order of the system is long range for $0 < x(Nb) \leq 0.04$, while orientational order decays within a few lattice constants for $x(Nb) \geq 0.07$. These data suggest that the CDW lattice evolves continuously from a crystalline solid, $x(Nb) = 0$, to a hexatic glass, $0 < x(Nb) \leq 0.04$, and finally to an amorphous state, $x(Nb) \geq 0.07$. Comparison of these results with equilibrium melting in 2D is discussed.

I. Introduction

Understanding the nature of the interaction between impurities and a charge density wave (CDW) is essential to understanding the static and dynamic properties of the CDW state.[1-6] In general, pinning can be defined as either strong or weak depending on the competing energetics of the CDW–impurity interaction and the CDW deformation energy.[1,3] In strong pinning the impurity potential dominates the CDW elastic energy and pins the phase of the CDW at each impurity site. In weak pinning the CDW breaks up into constant phase regions that are pinned collectively by impurities. Despite the fundamentally different structural manifestations of strong and weak pinning, there has been considerable controversy concerning the nature of pinning in CDW systems.[3-11] This controversy has been due in large part to the lack of direct data characterizing the evolution of CDW structure with impurity doping. Real-space imaging of the CDW structure in doped materials by scanning tunneling microscopy (STM) is, however, beginning to provide a direct method of addressing the essential issue of strong versus weak pinning.[10-13]

In addition, an important and general consequence of pinning is structural disorder. In two-dimensional (2D) systems disorder can manifest itself in intriguing ways.[14-18] For example, Halperin and Nelson predicted that a 2D solid can melt in a continuous transition through a hexatic state that is characterized by long-range orientational order and exponentially decaying positional order.[15] This unique hexatic state arises from the formation of topological defects, dislocations, in the lattice. Disorder due to impurity pinning has many similarities to melting, although the melting theory[14-16] is based upon equilibrium thermal disorder whereas pinning is typically a quenched disorder. Since statistical averaging differs for equilibrium and quenched disorder,[19] it is important to examine carefully the analogy of disorder in pinned systems to equilibrium theory.

In this study we have addressed the nature of CDW impurity pinning in Nb-doped TaS_2, $Nb_xTa_{1-x}S_2$, and have elucidated the detailed characteristics of disorder in this pinned CDW system. Real-space images of the CDW lattice as a function of Nb impurity concentration were obtained by STM and were quantitatively analyzed to determine the topological defects and the radial, translational, and orientational correlation functions. These data show unambiguously that CDW pinning by the Nb impurities is weak or collective. In addition, our work demonstrates that this system evolves through crystalline, hexatic glass, and amorphous states as a function of impurity concentration. A preliminary account of this work has appeared.[11]

II. Experimental Methods

Single crystals of $Nb_xTa_{1-x}S_2$ ($x = 0, 0.02, 0.04, 0.07, 0.1$) were grown by iodine vapor transport in a 70 °C gradient with a growth temperature of 870 °C.[13] Bulk and surface analyses were used to verify the concentration of Nb and the stoichiometry of the crystals. The incommensurate to nearly-commensurate CDW transition temperatures of these Nb-doped crystals were determined by four-probe resistivity measurements and found to agree with previous reports.[2,13] The transition temperatures for the $x(Nb) = 0$, 0.02, and 0.04 samples were 350, 330, and 320 K, respectively. The $x(Nb) = 0.07$ and 0.10 materials do not exhibit a transition; i.e., the samples remain in the incommensurate state.

Variable-temperature STM measurements were made with commercial instrument[20] that has been modified for operation at temperatures up to 420 K. The temperature was monitored using a calibrated thermocouple placed directly behind the sample. The system exhibits ±0.1 K temperature stability for >1 h. Images were acquired in the constant current mode on cleaved crystal surfaces using Pt–Ir alloy (80%–20%) tips. The images of the $x(Nb) = 0, 0.02, 0.04, 0.07$, and 0.10 single crystals were obtained at temperatures of 380, 360, 340, 315, and 298 K, respectively. For these imaging temperatures the samples are in the incommensurate CDW state. The digital STW images were analyzed using standard methods.[11,21,22] Briefly, the CDW maxima, which we call lattice sites, were located to ±1 pixel accuracy by a thresholding algorithm. These computer generated lattices were checked interactively with the original images before proceeding with the analysis. Typically, images 30–90 lattice constants on edge were examined, although the maximum number of lattice sites that could be used in our calculations was 4000. Other experimental details have been described previously.[11,13,20]

† Dedicated to Professor Dudley Herschbach on the occasion of his 60th birthday.

0022-3654/93/2097-2362$04.00/0

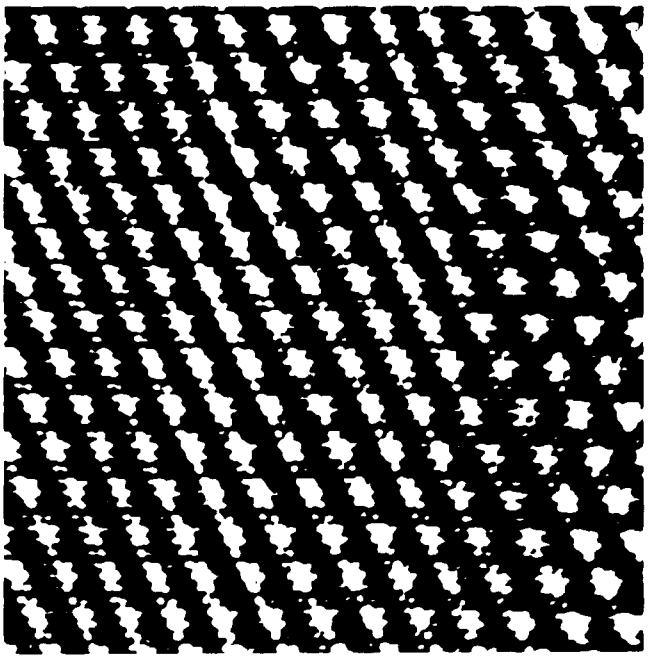

Figure 1. STM image of TaS_2 recorded at 360 K. The image exhibits both the atomic lattice (a = 3.35 Å) and the CDW superlattice (a = 11.8 Å).

III. Results and Discussion

A. STM Images and Topological Defects. High-resolution STM images of the $Nb_xTa_{1-x}S_2$ materials are shown in Figures 1–3. Images of the incommensurate CDW phase of undoped TaS_2 samples exhibit a well-ordered hexagonal CDW superlattice and atomic lattice (Figure 1). In contrast, substitution of Nb causes disorder in the CDW lattice (Figures 2 and 3). The images of the x(Nb) = 0.02 samples exhibit areas in which the CDW lattice has hexagonal order and also regions containing defects; these defects introduce disorder into the CDW lattice. The predominant defects observed in the samples containing x(Nb) $\leq$ 0.04 are dislocations. Dislocations are formed by the insertion of an extra half row of CDW sites in the lattice; black lines in Figure 2a highlight the creation of one dislocation. An important point to recognize about these defects is that there is a significant strain field at the dislocation.[23] The CDW can relax the strain field by locally deforming (i.e., rotating), although such local rotations create disorder.

As the impurity concentration increases to x(Nb) = 0.04, we find that dislocations appear with a higher density than in the x(Nb) = 0.02 samples (Figure 2b). The CDW lattice rows near the dislocation are deformed as discussed above. However, in areas free of dislocations the CDW lattice is locally ordered. We have highlighted several dislocation cores (the region where the CDW deforms) by constructing Burgers loops (Figure 2b). The Burgers loop consists of an equal number of steps along each lattice direction; the loop will remain open if it encloses a single dislocation. The vector pointing from start to end of the loop, the Burgers vector, uniquely defines the dislocation.[23] We find that the Burgers vectors defining the CDW dislocations in the Nb-doped samples occur along each of the three crystallographic axes, and thus we conclude that impurity-induced dislocations occur randomly in the CDW lattice. In the samples containing higher impurity concentrations, x(Nb) = 0.07 and 0.10, the STM images exhibit extended defects (Figure 3). The CDW lattice in these latter samples exhibits significant disorder with regions of hexagonal order extending only several lattice constants.

To elucidate in detail the topology and density of these defects, we have quantitatively analyzed the STM images. The quantitative analysis involves defining the x,y coordinates of each CDW maxima and the unique nearest neighbors in the lattice.

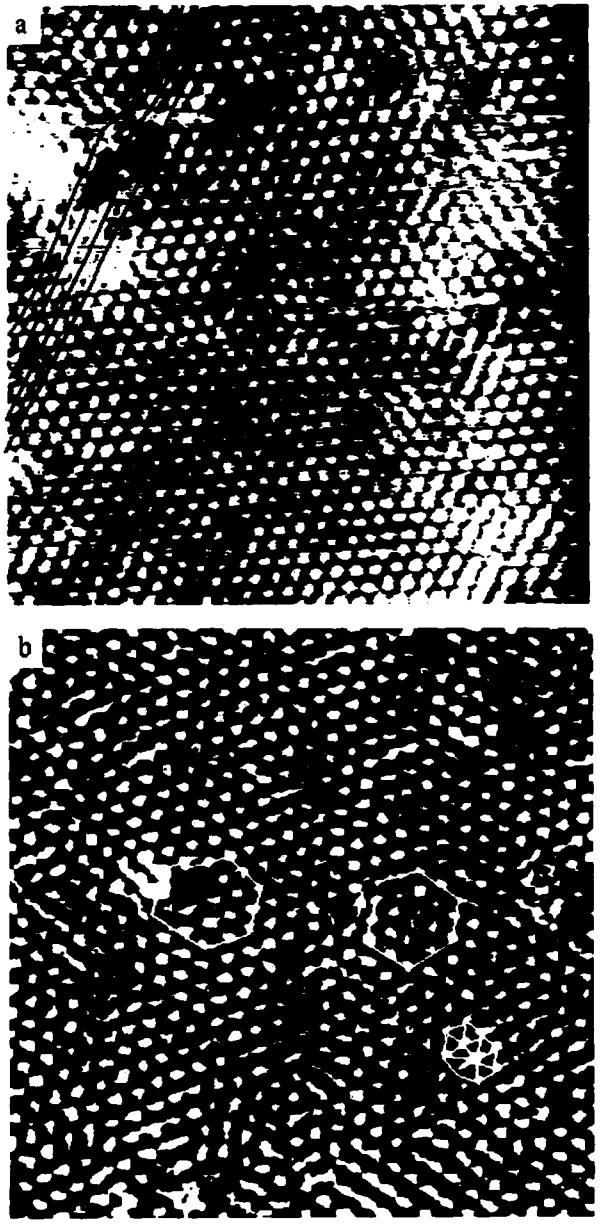

Figure 2. STM images of the incommensurate CDW state in (a) $Nb_{0.02}Ta_{0.98}S_2$ and (b) $Nb_{0.04}Ta_{0.96}S_2$. Black lines highlight the insertion of an extra row of CDW lattice sites in (a). Two distinct loops and Burgers vectors are drawn in (b) to highlight dislocations in the CDW lattice. A 5-fold–7-fold disclination pair is also shown in (b).

The CDW maxima, which we call lattice sites, were located to ±1 pixel accuracy by a thresholding algorithm. Once the lattice points are located, a sweep-line algorithm[24] is used to construct the Voronoi diagram for the lattice. The Voronoi diagram determines the nearest neighbors of all of the lattice points uniquely[25] and thus can be used to illustrate explicitly all topological defects in the lattice. To illustrate these defects, we triangulate the Voronoi diagram by drawing "bonds" from all CDW lattice points to their nearest neighbors. Hence, fully coordinated lattice sites are indicated by six bonds to the CDW maxima, while defects contain fewer or greater bonds. Typical results obtained from the analysis of x(Nb) = 0, 0.02, 0.04, 0.07, and 0.10 samples are shown in Figure 4. In these triangulations we have highlighted the defect (non-6-fold coordinate) sites by shading. Analyses of images recorded on pure TaS_2 show that the CDW lattice is free of topological defects; that is, all of the lattice sites are 6-fold coordinate (Figure 4a). The triangulations explicitly show, however, that the Nb-doped materials have topological defects in the CDW lattice. At low concentrations of impurities, x(Nb) = 0.02 and 0.04, we find that the dislocations

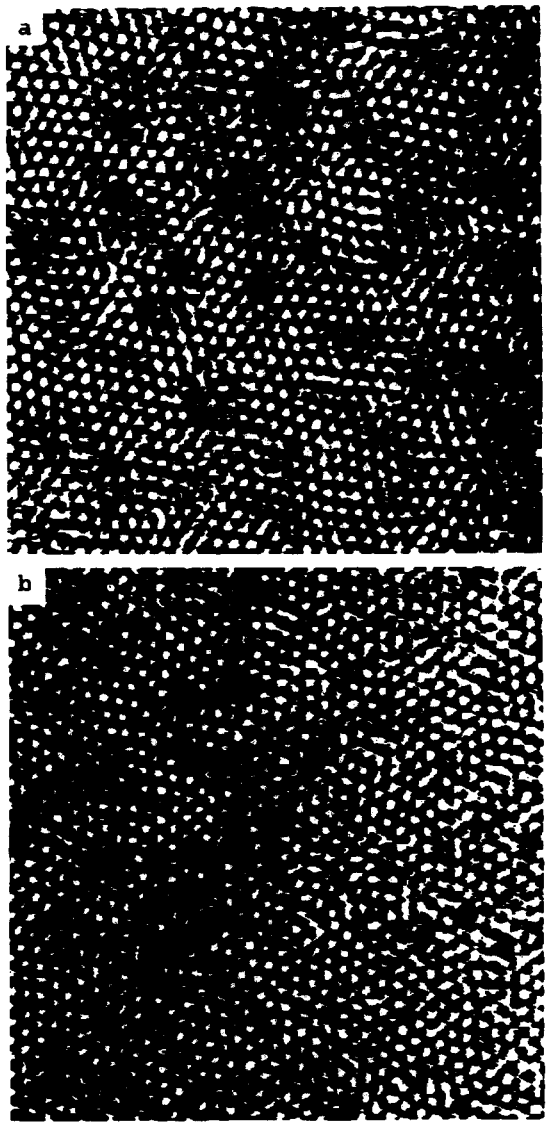

Figure 3. STM images of the incommensurate CDW phase in (a) $Nb_{0.07}Ta_{0.93}S_2$ and (b) $Nb_{0.1}Ta_{0.9}S_2$.

consist of 5-fold/7-fold disclination pairs (Figure 4b,c). Extended defect networks are also obvious in the triangulation data for the x(Nb) = 0.07 and 0.10 samples. These extended topological defects consist of dislocations and free disclinations.

We have also used this data to determine the separation between dislocations. We find that the average spacing between dislocations in the x(Nb) = 0.02, 0.04, 0.07, and 0.1 CDW lattices is 12, 8, 5, and 3 lattice constants, respectively. In comparison, the average separation between the Nb impurities in the lattice (d_i) is 0.80, 0.57, 0.43, and 0.36 CDW lattice constants, respectively. The average separation between dislocations is thus always greater than the average impurity spacing; that is, impurity pinning of the CDW must be a collective effect. Hence, these results strongly suggest that CDW pinning in the $Nb_xTa_{1-x}S_2$ materials is weak.

B. CDW Pinning. To further examine the issue of CDW pinning, we consider theoretical models of the CDW–impurity interaction. The one-dimensional model first proposed by Fukuyama, Lee, and Rice (FLR) has been the most widely studied example for CDW–impurity pinning.[3] For this one-dimensional model the CDW wave function is

$$\rho(x) = \rho_0 + \rho \cos(Qx + \phi(x)) \quad (1)$$

where $\rho(x)$ is modulated charge density, ρ_0 is the background charge density, ρ is the CDW amplitude, Q is the CDW wave vector, and $\phi(x)$ is the CDW phase. Analysis of this model shows that there are two distinct regimes which describe the strength of the CDW–impurity interaction (i.e., strong and weak pinning). These two regimes can be defined in terms of a competition between the pinning energy $E_p = V_0\rho$ and the CDW elastic energy $E_e = \alpha\kappa$. In strong pinning the impurity potential V_0 dominates the elastic energy: $\epsilon = V_0\rho/\alpha\kappa \gg 1$. Since the CDW is pinned to each impurity site in the lattice, the CDW phase undergoes abrupt changes at the impurity sites. Conversely, in weak pinning the CDW stiffness resists deformation by the impurity potential: $\epsilon \ll 1$. For weak pinning the total energy is minimized through collective interactions. Hence, the CDW phase can vary smoothly over a region containing many impurities.

The 2D CDW system studied here should form areas with local phase coherence and positional order if the system is weakly pinned. Dislocations and other defects will separate phase coherent regions. These locally coherent regions can be understood by scaling arguments. For an area of length scale L with impurity density n_i, the energy gain from pinning per unit area will be $V_0\rho(L^2n_i)^{1/2}L^{-2}$ while the elastic energy cost is $\sim\alpha\kappa L^{-2}$.[26,27] By minimizing the total energy density, one finds an optimized correlation length L_c

$$L_c = (2/\epsilon)d_i \quad (2)$$

where $d_i = (1/n_i)^{1/2}$ is the spacing between impurities. Within the length scale L_c, the CDW phase varies smoothly between $-\pi$ and π; positional correlations will only be sustained on a scale smaller than L_c. Alternatively, this scaling argument can be used to explain the formation of dislocations. The energy cost for a dislocation loop with size L is $\sim\alpha\kappa$ up to a logarithm,[23] while the energy gain due to pinning is $V_0\rho(L^2n_i)^{1/2}$. Hence, creating a dislocation on length scale larger than $L_c = (2/\epsilon)d_i$ is energetically favorable.

As shown in section A, the spacing between dislocations in the CDW lattice is significantly larger than the distance between Nb impurities.[11] This observation is consistent with the weak pinning model developed above. A related criteria for weak pinning is the presence of ordered regions with a critical size directly proportional to the impurity spacing. Notably, analysis of large area STM images demonstrates that areas of the CDW lattice that are free from dislocations exhibit a smooth variation in the CDW phase as we expect for the case of weak pinning. In Figure 5 several constant phase regions are highlighted to demonstrate this important point. Moreover, we can use our scaling equation to estimate the magnitude of the dimensionless parameter ϵ. Using the L_c determined from our images and the known impurity spacing, we find that $\epsilon = 0.1$–$0.2 \ll 1$. These results demonstrate that the CDW pinning in $Nb_xTa_{1-x}S_2$ is weak.

C. A Quantitative Analysis of Disorder. It is also important to examine the consequences of the disorder produce by weak pinning in this system. We first examine the structure factor, $S(k) = |\rho(k)|^2$, to investigate the average structural effects of pinning. $S(k)$'s were calculated from the square of the Fourier transform of the STM images; the results for the x(Nb) = 0.02, 0.04, 0.07, and 0.10 samples are shown in Figure 6. $S(k)$ for pure TaS_2 (not shown) exhibits sharp 6-fold symmetric peaks. These peaks broaden both radially and angularly as the impurity concentration increases to 0.04. For the x(Nb) = 0.07 and 0.10 the first-order Bragg peaks have broadened to form a ring whose intensity has a 6-fold modulation. The angular broadening is due to CDW rotations that were discussed above in section A. This broadening indicates a loss of orientational order; however, it is not possible to provide a quantitative measure of the orientational disorder from this $S(k)$ data. In addition, the radial widths of the Bragg peaks indicate that the translational correlation length is short in all of the Nb-doped materials. Notably, these $S(k)$ data are qualitatively similar to the results expected for 2D melting through a hexatic state.[10,21,22,28,29]

To provide a quantitative measure of the order in this system

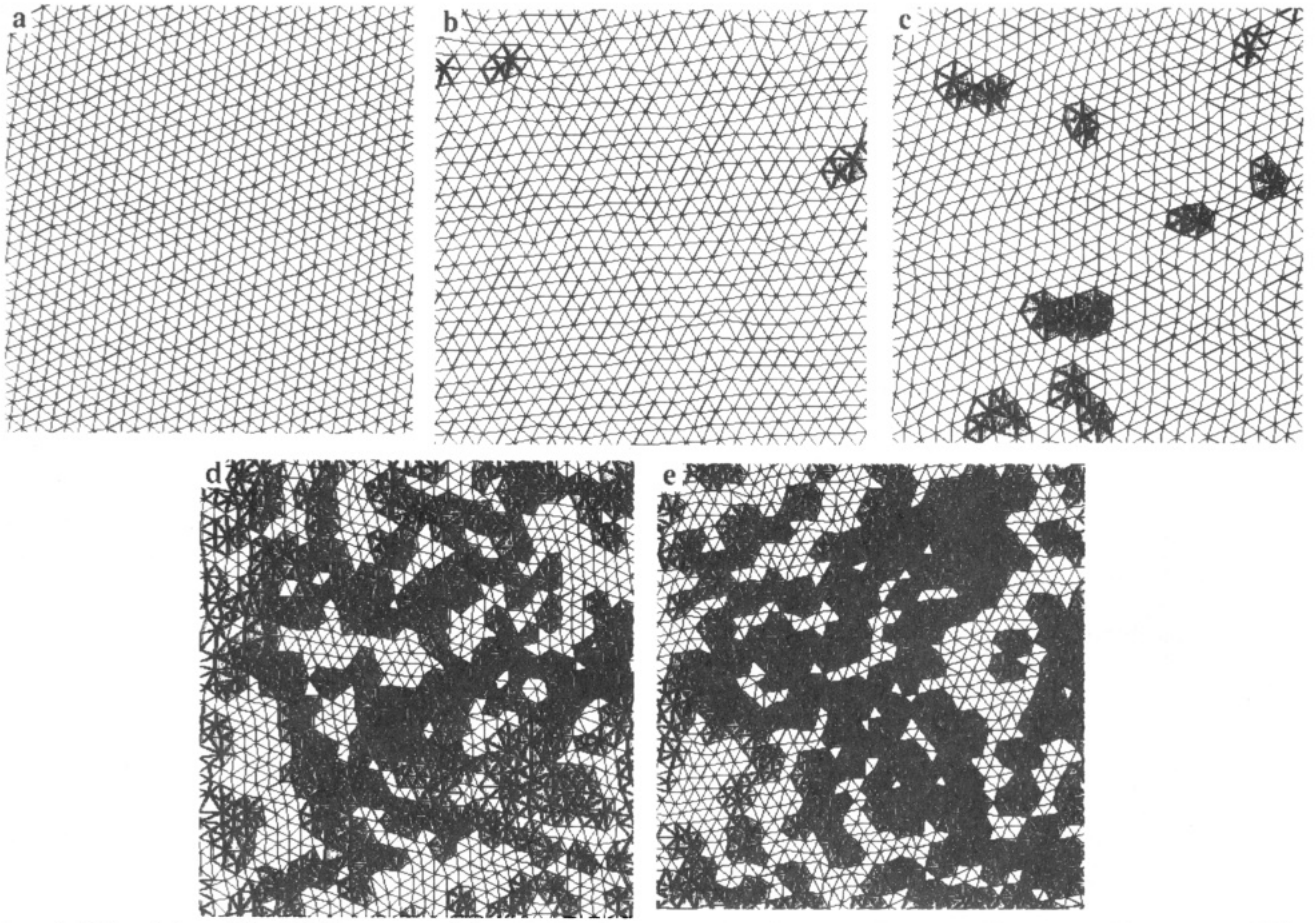

Figure 4. Triangulations of the STM images recorded on $Nb_xTa_{1-x}S_2$ crystals where (a) $x = 0$, (b) $x = 0.02$, (c) $x = 0.04$, (d) $x = 0.07$, and (e) $x = 0.10$. Lattice sites that do not have 6-fold coordination are highlighted by shading the triangles which have the non-6-fold coordinate site as a vertex.

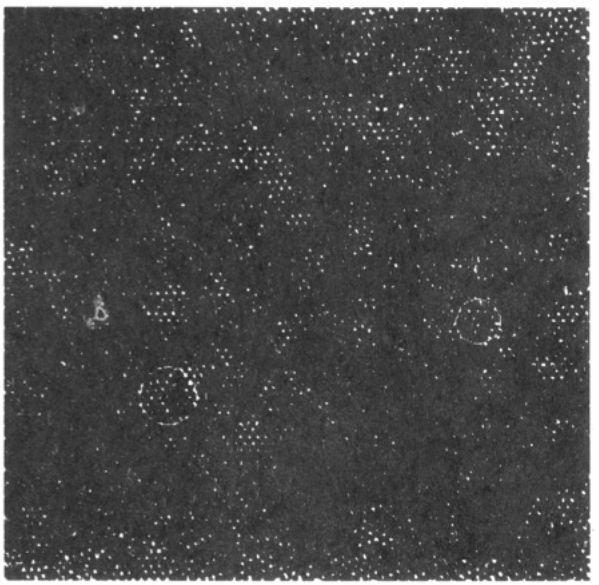

Figure 5. Large area STM image of the incommensurate CDW lattice of a $Nb_{0.07}Ta_{0.93}S_2$ sample. Two regions with good positional order are highlighted circles.

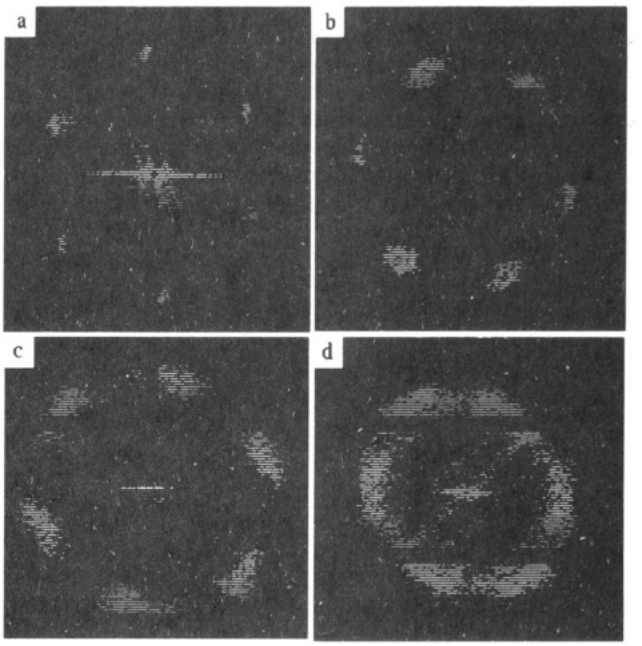

Figure 6. Structure factors corresponding to the CDW lattices of (a) $x = 0.02$, (b) $x = 0.04$, (c) $x = 0.07$, and (d) $x = 0.10$ $Nb_xTa_{1-x}S_2$ materials.

and how it is affected by impurity pinning, we have investigated the radial distribution, translational correlation, and orientational correlation functions. The radial distribution function is defined as $g(r) = \langle n(r) \rangle / N_0$, where $n(r)$ is the point density at distance r from the origin of the structure and N_0 is the average density of points. For a general structure, $g(r)$ tends to 1 as $r \rightarrow \infty$; that is, the distribution of points at large distances appears uniform. The results of the calculations of $g(r)$ are presented in Figure 7. For the x(Nb) = 0 sample $g(r)$ oscillates strongly out to more than 10 lattice constants. The persistent oscillation in $g(r)$ indicates that positional order is long range. When the impurity level increases to 0.02 and 0.04, the amplitude of the oscillations in $g(r)$ decreases and the oscillations die out much more rapidly than in $g(r)$ for the pure material (Figure 7, a vs b,c). For the x(Nb) = 0.07 or 0.1 materials the amplitude of the peaks in $g(r)$ is further reduced, and these peaks only persist to the second or

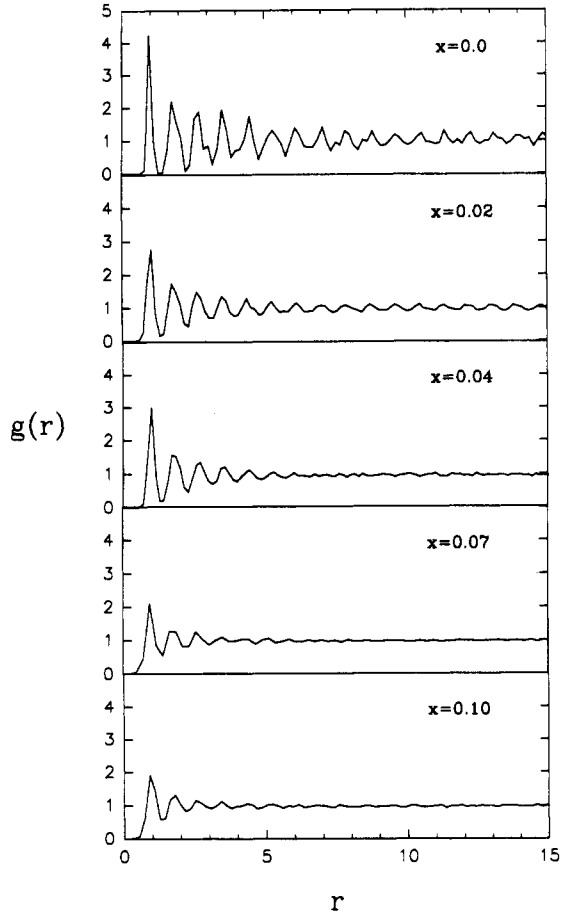

Figure 7. Radial distribution functions for the $x = 0$, $x = 0.02$, $x = 0.04$, $x = 0.07$, and $x = 0.10$ $Nb_xTa_{1-x}S_2$ materials. The x axis corresponds to CDW lattice constants.

third nearest neighbors. These results indicate that Nb impurities destroy translational order in this CDW system.

To further characterize the order of this 2D system, we have calculated the translational and orientational correlation functions. Previous theoretical work has shown that these functions provide a unique description of the order in 2D systems.[15,17] The translational correlation function is defined as $G_T(\vec{r}) = \langle\psi(0)\psi(\vec{r})^*\rangle$, where $\psi(\vec{r})$ is the translational order parameter at position r: $\psi(\vec{r}) = \sum_{i=1}^{3} \exp(i\vec{G}_i\vec{r})/3$. The summation is over the three reciprocal lattice vectors, G_L. The orientational correlation function is $G_6(\vec{r}) = \langle\psi_6(0)\psi_6(\vec{r})^*\rangle$, where $\psi_6(\vec{r})$ is the orientational order parameter: $\psi_6 = \sum_{i=1}^{N_i} \exp(i6\theta(\vec{r}))/N_i$. $\theta(\vec{r})$ is the bond angle with respect to a fixed direction, where the "bonds" are the lines that connect nearest neighbors as in the triangulation (Figure 4). N_i is the number of bonds at the ith point, and the summation is over all bonds at position r. For a perfect lattice $G_T(\vec{r}) = G_6(\vec{r}) = 1$.

Dislocations observed in the CDW lattice will reduce both $G_T(\vec{r})$ and $G_6(\vec{r})$, although the detailed effect on these functions is expected to be quite different. Qualitatively, a dislocation is very effective in destroying translational order since it displaces the CDW sites on the order of one lattice constant. Translational order should, therefore, only be sustained in regions free of dislocations. Indeed, Halperin and Nelson showed that when the structural order is dominated by dislocations, the translational correlation length is approximately equal to the dislocation spacing. In the case of $G_6(\vec{r})$ the effect of dislocations is expected to be quite different. For a dislocation consisting of a bound pair of 5-fold–7-fold disclinations (Figure 4), the bond orientational order parameters at these two points are obviously reduced. Because the disclinations are closely bound, they do not change the coordination number and orientation of points away from the dislocation. Hence, dislocations do not necessarily destroy orientational order.

The calculated results for $G_T(\vec{r})$ and $G_6(\vec{r})$ are shown in Figure 8. $G_T(\vec{r})$ and $G_6(\vec{r})$ decay very little over 20 lattice constants for the pure sample. However, all of the samples that contain Nb impurities exhibit a rapid decay of translational order. This decay in $G_T(\vec{r})$ can be fit reasonably well to an exponential of the form $G_T(\vec{r}) = \exp(-r/\xi_T)$, where ξ_T is the translational correlation length. The range of the ξ_T's determined by averaging a number of images are ξ_T = 7–10, 3–6, 2–3, and 1–2 lattice constants for the x(Nb) = 0.02, 0.04, 0.04, and 0.10 samples, respectively. The values of ξ_T are similar to the average dislocation spacing determined from triangulation data (e.g., Figure 4), and furthermore these results demonstrate quantitatively that weak pinning by the Nb impurities destroys translational order. In contrast, we find that the orientational correlations die out slowly for the 0.02 and 0.04 samples, although $G_6(\vec{r})$ decays rapidly for x(Nb) = 0.07 and 0.10 (Figure 8f–j). If the x(Nb) = 0.02, 0.04,

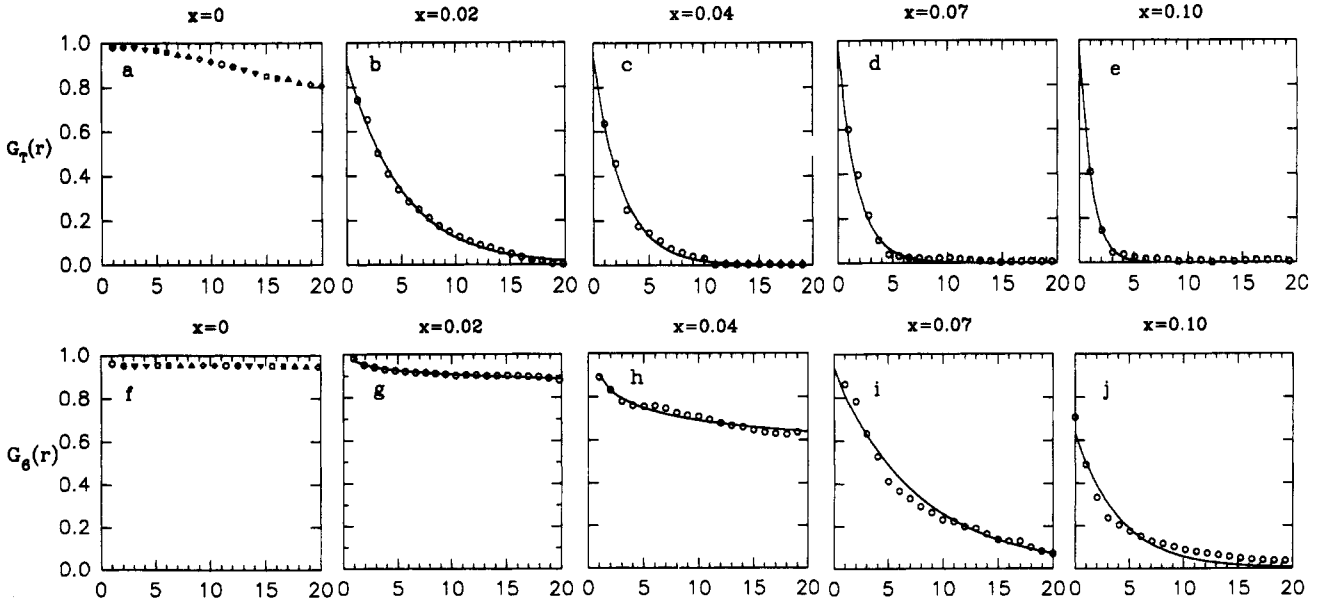

Figure 8. Translational correlation functions $G_T(r)$ (a–e) and orientational correlation functions $G_6(r)$ (f–j) calculated from images $x = 0$, 0.02, 0.04, 0.07, and 0.10 $Nb_xTa_{1-x}S_2$ materials. The x axes in these figures correspond to lattice constants. The points represent the experimental data, and the lines correspond to exponential ($e^{-r/\xi}$) fits (a–e) and (i, j) or power law ($r^{-\eta}$) fits (g, h).

0.07, and 0.10 data are fit with an exponential, $G_6(\vec{r}) = \exp(-r/\xi_6)$, we obtain correlation lengths of $\xi_6 \approx 200$, 100, 11, and 5 lattice constants, respectively. A better fit to $G_6(r)$ for $x(\mathrm{Nb}) = 0.02$ and 0.04 is obtained, however, using an algebraic decay, $G_6(\vec{r}) = r^{-\eta}$, with $\eta = 0.03$ and 0.12, respectively.

The simultaneous observation of long-range orientational order and short-range translational order in the $x(\mathrm{Nb}) = 0.02$ and 0.04 samples is strongly suggestive of the hexatic state that arises in 2D melting driven by topological defects.[15] 2D melting theory, which is based on equilibrium statistical mechanics, predicts that melting is a continuous phase transition between (1) a crystalline solid phase that has long-range translational and orientational order, $G_T(\vec{r}) \sim r^{-\xi}$, $G_6(\vec{r}) \sim 1$; (2) a hexatic phase that has short-range translational order but long-range orientation order, $G_T(\vec{r}) = e^{-r/\xi_T}$, $G_6(\vec{r}) \sim r^{-\eta}$; and (3) a liquid phase that has short-range translational and orientational order, $G_T(\vec{r}) = e^{-r/\xi_T}$, $G_6(\vec{r}) = e^{-r/\xi_6}$. Our data show similar behavior, and thus we suggest that the CDW lattice evolves from crystalline ($x = 0$) to hexatic ($x = 0.02$–0.04) to amorphous ($x \geq 0.07$) states. The important difference between the melting theory and our study is that the topological defects arise from thermal fluctuations in the former and from pinning to a quenched impurity distribution in our work. Since statistical averaging differs for equilibrium versus quenched disorder,[19] we investigate further the similarities of this pinned 2D CDW system to equilibrium melting.

First, we can estimate the power law exponent η using the relationship $\eta = 9c/\pi$, where c is a fractional area of dislocation cores, derived from equilibrium theory.[21] The values of η calculated in this way, 0.02 and 0.13, are in excellent agreement with the values obtained from fits to $G_6(\vec{r})$ for $x(\mathrm{Nb}) = 0.02$ and 0.04. This agreement strongly suggests that dislocations determine the orientational order. The average dislocation spacing (ξ_D) is also similar to ξ_T, although at the smallest impurity concentration ξ_D is always larger than ξ_T. This result indicates that dislocations are not the only factor that causes the short-ranged translational order in CDW lattice, in contrast to equilibrium melting. The fact that $\xi_T < \xi_D$ can be understood by weak pinning theory. As discussed above in section B, the CDW phase varies smoothly from $-\pi$ to π in the regions separated by dislocations. This smooth variation in phase also causes small distortions of the CDW lattice positions and will therefore reduce the translational order. In fact, Chudnovsky has explicitly shown how elastic distortions alone (i.e., smooth variations in the phase) destroy the positional order of impurity pinned lattices.[30] Hence, a combination of equilibrium melting theory and Chudnovsky's theory provides a better description of the changes in translational correlations for this pinned 2D CDW system.

IV. Conclusions

We have used STM and quantitative image analysis to elucidate systematically CDW pinning and disorder in $Nb_xTa_{1-x}S_2$ solids. Analyses of STM images demonstrate that Nb impurities introduce topological defects, dislocations, in the CDW lattice. Quantitative analysis of the density of dislocations and comparisons of this data with theoretical scaling arguments demonstrates unambiguously that the pinning of the CDW by Nb impurities is weak. In addition, we have shown how pinning affects the translational and orientational order of the 2D CDW lattice. Calculations of the translational correlation function demonstrate that translational order decays exponentially for $x(\mathrm{Nb}) > 0$ and thus that Nb impurities destroy translational order in this system. In contrast, calculations of the orientational correlation function showed for $0 < x(\mathrm{Nb}) \leq 0.04$ that the orientational order of this the system is long range, while for $x(\mathrm{Nb}) \geq 0.07$ orientational order decays within a few lattice constants. These calculations thus suggest that the CDW lattice evolves continuously from a crystalline solid, $x(\mathrm{Nb}) = 0$, to a hexatic glass, $0 < x(\mathrm{Nb}) \leq 0.04$, and finally to an amorphous state, $x(\mathrm{Nb}) \geq 0.07$. Finally, we have shown that the structural evolution of the CDW lattice with increasing impurity concentration has many analogous features to equilibrium melting in 2D, although there are differences that we believe arise from the quenched disorder and pinning in $Nb_xTa_{1-x}S_2$. In the future further experimental and theoretical investigations of this system will undoubtably lead to a much deeper understanding of pinning and nonequilibrium disorder in 2D systems.

References and Notes

(1) (a) Gruner, G. *Rev. Mod. Phys.* **1988**, *60*, 1129. (b) Gruner, G.; Zettl, A. *Phys. Rep.* **1985**, *119*, 117.
(2) (a) Wilson, J. A.; DiSalvo, F. J.; Mahajan, S. *Adv. Phys.* **1975**, *24*, 117. (b) DiSalvo, F. J.; Wilson, J. A.; Bagley, B. G.; Waszczak, J. V. *Phys. Rev. B* **1975**, *12*, 2220.
(3) (a) Fukuyama, H.; Lee, P. A. *Phys. Rev. B* **1978**, *17*, 535. (b) Lee, P. A.; Rice, T. M. *Ibid.* **1979**, *19*, 3970.
(4) Coopersmith, S. N. *Phys. Rev. Lett.* **1990**, *65*, 1044.
(5) Tucker, J. R. *Phys. Rev. B* **1989**, *40*, 5447.
(6) Bardeen, J. *Phys. Rev. Lett.* **1990**, *64*, 2297.
(7) Sweetland, E.; Tsai, C.-Y.; Wintner, B. A.; Brock, J. D.; Thorne, R. E. *Phys. Rev. Lett.* **1990**, *65*, 3165.
(8) (a) Tucker, J. R. *Phys. Rev. Lett.* **1990**, *65*, 270. (b) Gill, J. C. *Phys. Rev. Lett.* **1990**, *65*, 271.
(9) Thorne, R. E.; McCarten, J. *Phys. Rev. Lett.* **1990**, *65*, 273.
(10) Dai, H.; Chen, H.; Lieber, C. M. *Phys. Rev. Lett.* **1991**, *66*, 3183.
(11) Dai, H.; Lieber, C. M. *Phys. Rev. Lett.* **1992**, *69*, 1576.
(12) Wu, X. L.; Lieber, C. M. *Phys. Rev. B* **1990**, *41*, 1239.
(13) (a) Wu, X. L.; Zhou, P.; Lieber, C. M. *Phys. Rev. Lett.* **1988**, *61*, 2604. (b) Chen, H.; Wu, X. L.; Lieber, C. M. *J. Am. Chem. Soc.* **1990**, *112*, 3326.
(14) Kosterlitz, J. M.; Thouless, D. J. *J. Phys. C.* **1973**, *6*, 1181.
(15) (a) Halperin, B. I.; Nelson, D. R. *Phys. Rev. Lett.* **1978**, *4*, 121. (b) Nelson, D. R.; Halperin, B. I. *Phys. Rev. B* **1979**, *19*, 2457.
(16) Young, A. P. *Phys. Rev. B* **1979**, *19*, 1985.
(17) Nelson, D. R. In *Phase Transitions and Critical Phenomena*; Domb, C., Lebovitz, J. L., Eds.; Academic Press: London, 1983; Vol. 7, p 1.
(18) Strandburg, K. J. *Rev. Mod. Phys.* **1988**, *60*, 161.
(19) Ma, S.-K. *Modern Theory of Critical Phenomena*; Benjamin/Cummings: Reading, MA, 1976.
(20) Nanoscope, Digital Instruments, Inc., Goleta, CA.
(21) Nelson, D. R.; Rubinstein, M.; Spaepen, F. *Philos. Mag. A* **1982**, *46*, 105.
(22) Murray, C. A.; Sprenger, W. O.; Wenk, R. A. *Phys. Rev. B* **1990**, *42*, 688.
(23) Nabarro, F. R. N. *Theory of Dislocations*; Clarendon: Oxford, 1967.
(24) Fortune, S. *Alforithmica* **1987**, *2*, 153.
(25) Voronoi, G. F. *J. Reine Agnew. Math.* **1908**, *134*, 198.
(26) Since $\alpha \sim L^{d-2}$ it will be of order unity for $d = 2$.
(27) Imry, Y.; Ma, S.-K. *Phys. Rev. Lett.* **1975**, *35*, 1399.
(28) Seshadri, R.; Westervelt, R. M. *Phys. Rev. Lett.* **1991**, *66*, 2774.
(29) Murray, C. A.; Gammel, P. L.; Bishop, D. J.; Mitzi, D. B.; Kapitulnik, A. *Phys. Rev. Lett.* **1990**, *64*, 2312.
(30) (a) Chudnovsky, E. M. *Phys. Rev. B* **1989**, *40*, 11355. (b) Chudnovsky, E. M. *Phys. Rev. B* **1991**, *43*, 7831.